ACS APPLIED MATERIALS & INTERFACES

Research Article

www.acsami.org

Intrinsically Mn^{2+}-Chelated Polydopamine Nanoparticles for Simultaneous Magnetic Resonance Imaging and Photothermal Ablation of Cancer Cells

Zhao-Hua Miao,[†,‡] Hui Wang,[§] Huanjie Yang,[§] Zheng-Lin Li,[∥] Liang Zhen,[†,‡] and Cheng-Yan Xu*[,†,‡]

[†]School of Materials Science and Engineering, Harbin Institute of Technology, Harbin 150001, People's Republic of China

[‡]MOE Key Laboratory of Micro-System and Micro-Structures Manufacturing, Harbin Institute of Technology, Harbin 150080, People's Republic of China

[§]School of Life Science and Technology, Harbin Institute of Technology, Harbin 150080, People's Republic of China

[∥]Condensed Matter Science and Technology Institute, School of Science, Harbin Institute of Technology, Harbin 150000, People's Republic of China

Supporting Information

ABSTRACT: Theranostic agents for magnetic resonance imaging (MRI) guided photothermal therapy have attracted intensive interest in cancer diagnosis and treatment. However, the development of biocompatible theranostic agents with high photothermal conversion efficiency and good MRI contrast effect remains a challenge. Herein, PEGylated Mn^{2+}-chelated polydopamine (PMPDA) nanoparticles were successfully developed as novel theranostic agents for simultaneous MRI signal enhancement and photothermal ablation of cancer cells, based on intrinsic manganese-chelating properties and strong near-infrared absorption of polydopamine nanomaterials. The obtained PMPDA nanoparticles showed significant MRI signal enhancement for both in vitro and in vivo imaging. Highly effective photothermal ablation of HeLa cells exposed to PMPDA nanoparticles was then achieved upon laser irradiation for 10 min. Furthermore, the excellent biocompatibility of PMPDA nanoparticles, because of the use of Mn^{2+} ions as diagnostic agents and biocompatible polydopamine as photothermal agents, was confirmed by a standard MTT assay. Therefore, the developed PMPDA nanoparticles could be used as a promising theranostic agent for MRI-guided photothermal therapy of cancer cells.

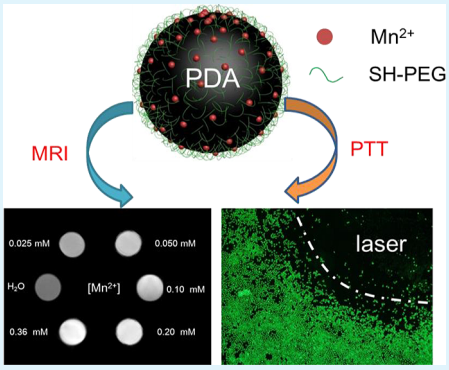

KEYWORDS: *polydopamine nanoparticles, theranostic agent, photothermal ablation, magnetic resonance imaging, cancer cells*

1. INTRODUCTION

Theranostic agents, consisting of diagnostic components and therapeutic components, have attracted intensive interest in the past decade. Diagnostic components can improve the knowledge of a disease state while therapeutic components improve the outcome of a disease state, and nanoparticles are good carriers for imaging and therapeutic components because of their intense and stable output, large payload delivery, and strong target binding via multiple ligands.[1] With the integration of contrast and therapeutic agents into a single nanoparticle, not only the location and size of diseased tissues can be easily detected before therapy but also the treatment procedure can be effectively monitored during therapy.[2] Several kinds of multifunctional nanocomposites as theranostic agents have been developed to more effectively conquer diseases and minimize side effect, such as FeCo/graphitic carbon, graphene oxide–Fe_3O_4, Fe_3O_4@Au, and gold-nanoshelled microcapsules.[2−5] These theranostic agents have shown great potential applications in cancer diagnosis and therapy.

Among numerous theranostic agents, nanocomposites for the integration of magnetic resonance imaging (MRI) and photothermal therapy (PTT) are quite fascinating. PTT is a new noninvasive treatment technique, which employs photoabsorbers to convert light energy into thermal energy to "heat" tumor cells.[6] Magnetic resonance imaging, as the preferred imagery technique in clinical practice, can provide excellent soft-tissue morphological details and functional information on lesions with high spatial resolution.[7] Besides, MRI can also estimate real-time temperature changes of cancer tissues during PTT procedure.[8] Therefore, it is essential to combine these two techniques together for cancer treatment. However, the design of theranostic agents for MRI-guided phototherapy remains a challenge. The majority of currently used therapeutic components are inorganic nanomaterials, such as Au nanoshells, Au nanorods, graphene oxide, and CuS nanoparticles,[9]

Received: December 22, 2014
Accepted: July 21, 2015
Published: July 21, 2015

DOI: 10.1021/acsami.5b06265
ACS Appl. Mater. Interfaces 2015, 7, 16946−16952

which are usually nonbiodegradable and remain in the body for long periods of time, raising the concerns of potential long-term toxicity.[10] On the other hand, although paramagnetic Gd chelates, manganese complexes, and superparamagnetic iron oxide nanoparticles have been reported as MRI agents, the study of manganese-enhanced MRI contrast agents, which have lower intrinsic toxicity than Gd^{3+}, has lagged far behind.[11] Compared with Gd-based agents that were recently involved in nephrogenic systemic fibrosis (NSF), Mn-based contrast agents often suffer from lower relaxivity coefficient.[12] And for T_1 MRI contrast agents, extrinsic chelators like DTPA (diethylenetriaminepentaacetic acid) or DOTA (1,4,7,10-tetraazacyclododecane-*N*,*N*′,*N*,*N*′-tetraacetic acid) are often needed to chelate Gd^{3+} or Mn^{2+} ions.[13] Very recently, Mn^{3+} incorporated porphysome as a new theranostic agent for the combination of manganese-enhanced MRI diagnosis and photothermal therapy has been reported,[14] but its relaxivity coefficient (1.2 mM^{-1} s^{-1}) is relatively low. Therefore, more attention should be paid to the design of novel theranostic agents with excellent biocompatibility, high photothermal conversion efficiency, and good MRI contrast effect.

Polydopamine (PDA), a major pigment of naturally occurring melanin (eumelanin),[15] has recently been reported as a photothermal agent because of good biocompatibility in vivo, high photothermal conversion efficiency (up to 40%), and strong optical absorbance in the near-infrared (NIR, wavelength = 700−1100 nm) region, where the absorption of body tissues is minimal and the penetration is optimal.[16,17] Chen and co-workers designed Fe_3O_4@PDA core−shell nanocomposites for multimodal imaging-guided photothermal therapy.[18] In addition, rich functional groups (i.e., catechol, carboxyl, and amino) in PDA or natural melanin endow their ability of directly cheating various metal ions including Fe^{3+}, Cu^{2+}, Ti^{4+}, and Mn^{2+} ions.[15,19] Despite melanin-based materials complexed with Gd^{3+} or Fe^{3+} ions have been reported as MRI contrast agents,[20,21] the trial of Mn^{2+}-chelated polydopamine nanoparticles as alone contrast agents or theranostic agents has not been reported so far.

In this article, we demonstrate, for the first time, that PEGylated Mn^{2+}-chelated polydopamine nanoparticles (denoted as PMPDA NPs) can serve as a novel theranostic agent for simultaneous magnetic resonance (MR) imaging and photothermal therapy of cancer cells. Compared with other theranostic agents,[22−24] PEGylated Mn^{2+}-chelated polydopamine nanoparticles as novel theranostic agents have several advantages: (1) No extrinsic chelators were needed to chelate Mn^{2+} ions because of intrinsic chelating properties of polydopamine nanomaterials. (2) By employment of Mn^{2+} ions as diagnostic agents and biocompatible polydopamine as photothermal agents, the PMPDA nanoparticles have low toxicity. (3) The fabrication procedure was very simple and safe without the requirement of high temperature or toxic reagents. These features ensure that PMPDA nanoparticles are more competitive than other theranostic agents for MRI-guided phototherapy.[22−24]

2. EXPERIMENTAL SECTION

2.1. Materials. Dopamine hydrochloride (98%) was supplied by Sigma-Aldrich (USA). Thiol−polyethylene glycol (SH-PEG, molecular weight 2000 Da) was purchased from Shanghai Yarebio, Co., Ltd. (China). $MnSO_4·H_2O$ (analytical reagent), ethanol (analytical reagent), and $NH_3·H_2O$ (28−30%) were all obtained from Sinopharm Chemical Reagent Co., Ltd. (China). Deionized water in the experiments was obtained by using a Milli-Q water system.

2.2. Synthesis of PDA Nanoparticles. The preparation of PDA nanoparticles with average diameter of 160 nm was according to the previous literature.[17] Typically, 1 mL of ammonia aqueous solution was mixed with 20 mL of ethanol and 45 mL of deionized water for 20 min under stirring at 30 °C. Then, 5 mL of dopamine hydrochloride solution (50 mg/mL) was quickly added into the above mixture solution. In 1 min, the color of solution turned to pale yellow. After vigorous stirring for 24 h, the resulting solution became dark brown. At last, PDA nanoparticles were obtained by centrifugation and washed with deionized water three times. For the synthesis of 70 and 300 nm PDA nanoparticles, the amount of ammonia aqueous solution was adjusted to 1.5 and 0.5 mL, respectively.

2.3. Preparation of Mn^{2+}−PDA Nanoparticles. The preparation of Mn^{2+}−PDA nanoparticles was as follows. An amount of 1 mL of $MnSO_4·H_2O$ solution (0.12 M) was added to 40 mL of PDA nanoparticles suspension (1 mg mL^{-1}). After vigorous stirring for 3 h, the Mn^{2+}−PDA nanoparticles were obtained by centrifugation and washed with deionized water at least five times to completely remove the residual Mn^{2+}.

2.4. Surface Modification of Mn^{2+}−PDA Nanoparticles by SH-PEG Molecules. For PEG modification, 100 mg of thiol−polyethylene glycol (SH-PEG) was added to 40 mL of Mn^{2+}−PDA nanoparticles suspensions (1 mg mL^{-1}). After stirring for 5 min, 0.2 mL of $NH_3·H_2O$ (28−30%) was then added to the above solution. After vigorous stirring for another 1 h, the PEGylated Mn^{2+}−PDA nanoparticles were obtained by centrifugation and washed with deionized water three times.

2.5. Characterization of PMPDA Nanoparticles. The morphology of PMPDA nanoparticles was observed using transmission electron microscope (TEM, JEOL JEM-2100) and scanning electron microscope (SEM, FEI Quanta 200F). The ζ potentials of the nanoparticles at different fabrication stages were measured using a PALS/90Plus instrument (Brookhaven Instruments Co., U.S.A). The optical spectra of PMPDA nanoparticles were acquired by the Shimadzu UV-2550 spectrophotometer. The FTIR spectra of nanoparticles were performed using a Varian 3000 FTIR in the range from 400 to 4000 cm^{-1}. The manganese concentration of PMPDA nanoparticles was determined by inductively coupled plasma atomic emission spectroscopy (ICP-AES). The release of Mn^{2+} ions from PMPDA nanoparticles was conducted by incubating PMPDA nanoparticles in PBS solution (pH = 7.4). The PMPDA suspensions were placed in a dialysis bag and then were dialyzed against 30 mL of PBS. At a certain time, the concentration of Mn^{2+} ions was measured by ICP-AES.

2.6. In Vitro and in Vivo MR Imaging. T_1-weighed imaging in vitro of PMPDA suspensions was conducted under a 9.4 T MRI scanner (Bruker Avance II 500WB, Germany). The PMPDA nanoparticles were dispersed in aqueous solution with Mn^{2+} concentrations from 0.025 to 0.36 mM. Pure water was used as negative control. The parameters were as follows: TR/TE = 1000/8.5 ms, flip angle = 180°, slice thickness = 1.5 mm. The relaxivity coefficients of PMPDA nanoparticles with the same concentration were also measured under a 1.5 T MRI sanner (HT-MRSI65-35, China). For in vivo MR imaging, nude mouse bearing 4T1 tumor was used as a model. An amount of 0.1 mL of PMPDA suspension (5 mg/mL) was injected into nude mouse through intravenous tail injection. T_1-weighed images were acquired with the 9.4 T MRI scanner (Bruker Avance II 500WB, Germany) at different time periods. The parameters were as follows: FOV = 160 mm, slice thickness = 1 mm.

2.7. Cytotoxicity Assay. MTT assay was applied to evaluate cytotoxicity using human umbilical vein endothelial cells (HUVECs) as a model. The cells were seeded in 96-well plate at a density of 1×10^4 cells per well for 24 h, followed by another 24 h incubation in fresh medium containing PMPDA nanoparticles with different concentrations (0, 10, 20, 40, 80, 160, 320 μg mL^{-1}). MTT was added to each well at a final concentration of 1 mg/mL, and the plate was incubated for 4 h at 37 °C to allow the formation of formazan dye. The formazan product was then dissolved in DMSO, and the absorbance of the

DOI: 10.1021/acsami.5b06265
ACS Appl. Mater. Interfaces 2015, 7, 16946−16952

solution was measured at 570 nm with a microplate reader (Infinite 200 NanoQuant, TECAN).

2.8. Measurement of Photothermal Effect. To study the photothermal effect, an amount of 3 mL of PMPDA nanoparticles with different concentrations (0−400 μg/mL) was suspended in quartz well and was exposed to an 808 nm laser with an output power of 2 W for 10 min. The temperature of the solutions was measured by a digital thermometer with a thermocouple probe every 10 s. For PDA and Mn^{2+}−PDA nanoparticles, the same procedure was conducted to evaluate their photothermal effects.

2.9. In Vitro Photothermal Ablation of HeLa Cells. HeLa cells were incubated with 100 μg/mL PMPDA dispersions for 4 h in a six-well plate and then irradiated by a NIR laser (808 nm, 6 W cm^{-2}) for 10 min. After the treatment, calcein AM was used to stain HeLa cells for visualization of living cells. The digital images of cells were then obtained by a fluorescence microscope.

To quantitatively evaluate the photothermal cytotoxicity of PMPDA NPs, a standard MTT assay was conducted as described above with minor modification. Briefly, after treatment with PMPDA nanoparticles (0, 10, 20, 40, 80, 160 μg mL^{-1}) for 4 h, cells were irradiated by using a NIR laser (808 nm, 6 W cm^{-2}) for 10 min. The cell viabilities were determined by a standard MTT assay.

3. RESULTS AND DISCUSSION

3.1. Synthesis and Characterization of PEGylated Mn^{2+}−PDA Nanoparticles. The synthetic procedure of PMPDA NPs is illustrated in Figure 1. PDA nanoparticles

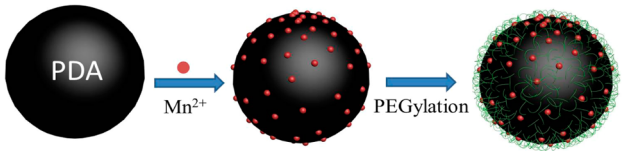

Figure 1. Schematic illustration of the fabrication of PEGylated Mn^{2+}−PDA nanoparticles.

were first synthesized via the polymerization of dopamine under alkaline environment.[25] The diameter of PDA nanoparticles can be easily tuned from 70 to 300 nm by changing the amounts of ammonium hydroxide (Figure S1c and Figure S1d). PDA nanoparticles with an average diameter of 160 nm were used for further experiments in this work. Then, $MnSO_4$ solution was mixed with PDA nanoparticles suspension, forming intrinsically Mn^{2+}-chelated nanoparticles without the assistance of any extrinsic chelators. The stable chelating was mainly derived from the coordination effect between Mn^{2+} ions and catechol or carboxyl groups in PDA nanoparticles.[26] To further increase the blood circulation time and biocompatibility, the surface of Mn^{2+}−PDA NPs was modified by thiol−polyethylene glycol (SH-PEG) molecules. The binding between thiol groups and the surface of PDA NPs is a covalent bond. At weak alkaline conditions, catechol groups in PDA equilibrate to *o*-quinones that are extremely reactive to thiols via Michael addition.[27,28] Typical SEM and TEM images (Figure 2a and Figure 2b) revealed that the obtained PEGylated Mn^{2+}−PDA nanoparticles were spherical and had an average diameter of 160 nm with a narrow size distribution, and the PDA or Mn^{2+}−PDA nanoparticles had the same morphology and size (Figure S1a and Figure S1b). This showed that the chelation of Mn^{2+} ions or SH-PEG modification would not change the morphology and size of PDA nanoparticles. Dynamic light scattering (DLS) data revealed that the hydrodynamic sizes of PDA, Mn^{2+}−PDA, PMPDA were 230.4 ± 3.8, 219.6 ± 3.2, 228.8 ± 4.7 nm,

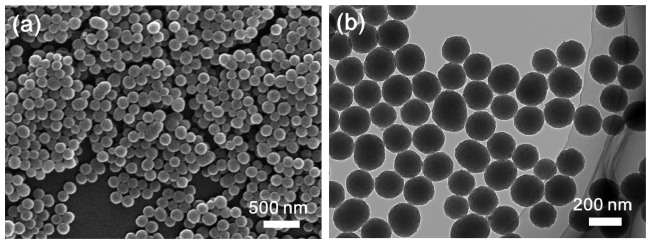

Figure 2. SEM image (a) and TEM image (b) of PMPDA NPs synthesized by the addition of 1 mL of ammonium hydroxide.

respectively. These values are larger than the average diameters determined by TEM. This is because the morphology of nanoparticles observed using TEM was obtained in dry and high vacuum environment while the hydrodynamic diameter is the sum of the core size and the thickness of surrounded water molecules.[29,30]

Unlike natural melanin, small PDA nanoparticles were highly dispersible and stable in both water and blood serum solution as previously reported.[17] The reason may be partly attributed to their high ζ potential. The ζ potential of pristine PDA nanoparticles was −12.04 ± 1.4 mV, due to the functional catechol groups. After mixing with positive Mn^{2+} ions, the surface charge changed to −5.20 ± 3.28 mV, indicating that Mn^{2+} ions were successfully chelated by PDA nanoparticles. When the surface of Mn^{2+}−PDA was further modified by highly negative SH-PEG, the surface charge was −27.43 ± 1.73 mV, which is high enough to ensure excellent colloidal stability. The change of ζ potential upon the binding of SH-PEG was similar to that of previously reported iron oxide nanoparticles modified by SH-PEG.[31]

Fourier transform infrared (FTIR) spectra were also conducted to confirm the binding of SH-PEG on the surface of PMPDA NPs. As shown in Figure S2, the characteristic peaks of SH-PEG at 2924 cm^{-1}, 2870 cm^{-1} (alkyl C−H stretching), and 1134 cm^{-1} (C−O−C stretching) were observed for PMPDA nanoparticles.[17,32] The bands of PDA nanoparticles appearing at 1509, 1599, and 3250 cm^{-1} were ascribed to the N−H bending vibrations, C═C resonance vibrations in the aromatic ring, and N−H/O−H stretching vibrations, respectively.[33,34] In addition, the manganese concentration as well as the number of Mn^{2+} ions per PMPDA nanoparticle was measured by ICP-AES. On the basis of the assumption that the average diameter of PMPDA nanoparticles was 160 nm and ICP-AES results, the estimated number of Mn^{2+} ions per nanoparticle was 1.22×10^5 by theoretical calculation, which was about 3−4 times higher than that of previously reported Gd^{3+}-based theranostic agents (3.5×10^4 Gd^{3+} per nanoparticle) with the same size.[35] The number of Mn^{2+} ions per Mn^{2+}−PDA nanoparticle was also calculated to be 1.24×10^5 with the same method, indicating that the binding of SH-PEG almost did not displace Mn^{2+} ions. Further stability assay of PMPDA showed that only about 8% Mn^{2+} ions were released from these nanoparticles in PBS after 48 h of incubation, indicating the stable chelating between Mn^{2+} ions and PDA nanoparticles (Figure S5).

3.2. In Vitro and in Vivo MR Imaging. The MRI contrast between normal and interest tissues, based on the tissue-dependent distributions of water molecules, can be increased by administration of a contrast agent before imaging.[36] To demonstrate the potential use of PMPDA nanoparticles as a novel MRI contrast agent, T_1-weighed imaging of PMPDA

DOI: 10.1021/acsami.5b06265
ACS Appl. Mater. Interfaces 2015, 7, 16946−16952

suspensions was conducted under a 9.4 T MRI scanner. As shown in Figure 3a, the image spots became brighter with the

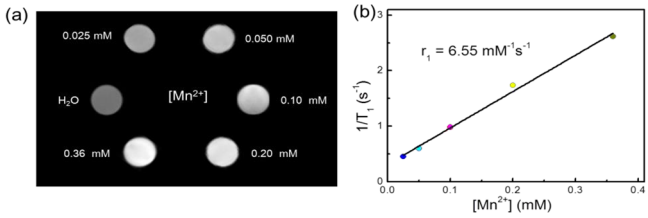

Figure 3. MRI in vitro assay of PMPDA NPs: (a) T_1-weighed images of water and PMPDA NPs in aqueous solution with Mn^{2+} concentrations of 0.025, 0.050, 0.10, 0.20, and 0.36 mM; (b) corresponding T_1 relaxation rate of the PMPDA NPs as a function of Mn^{2+} concentration.

increase of Mn^{2+} ion concentration from 0 to 0.36 mM, indicating the significant increase of the T_1 signal intensity. The longitudinal relaxivity coefficient (r_1) of PMPDA NPs was calculated to be 6.55 mM^{-1} s^{-1} (Figure 3b), higher than that of the commercially available agent Gd-DTPA (3.71 mM^{-1} s^{-1} at 9.4 T).[37] Meanwhile, the relaxivity coefficients of PMPDA nanoparticles were also measured under a 1.5 T MRI scanner. As shown in Figure S6, r_1 is up to 38.6 mM^{-1} s^{-1}, and the corresponding transverse relaxivity coefficient (r_2) was 104.2 mM^{-1} s^{-1} at 1.5 T. As expected, the value of r_1 increased rapidly with the decrease of magnetic field strength, and this phenomenon was similar to some previous reports.[38,39] The significant enhancement in relaxivity for T_1-weighed MRI may be attributed to its characteristic catechol or carboxyl groups, which enable more water molecules to bond to Mn^{2+} complex.[21] To be addressed, the use of Mn^{2+} rather than Gd^{3+} for MRI signal enhancement can avoid the risk of nephrogenic systemic fibrosis in clinical practice. The in vivo MRI experiment was conducted at 9.4 T. The MR images of mouse bearing 4T1 tumor were acquired before and after the intravenous tail injection of PMPDA NPs (0.1 mL, 5 mg/mL). As shown in Figure 4, a detectible T_1-weighed contrast

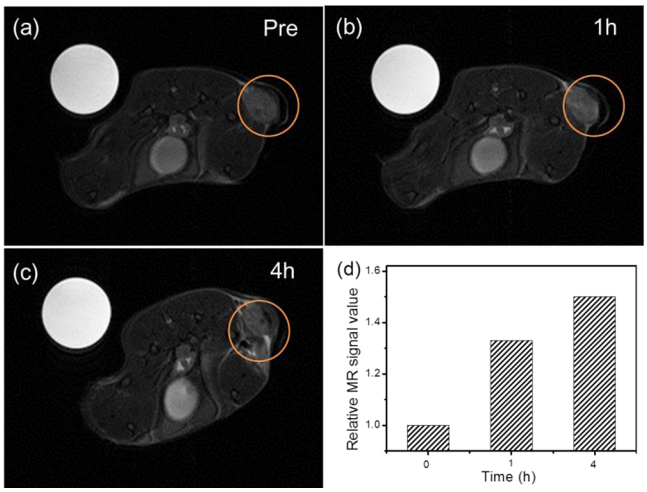

Figure 4. (a–c) In vivo T_1-weighed MR imaging of 4T1 tumor bearing-mouse at different time after the intravenous tail injection of PMPDA NPs. The orange circles indicate tumor issues. The big white spots in the top-left corner are pure water as background. (d) Corresponding normalized signal intensity of T_1-weighted MR signals from the tumor at different time.

enhancement was observed in the tumor area (marked by orange circles) 1 h after injection. The enhancement effect was more obvious at 4 h after injection, and quantitative analysis indicated that the MR signal intensity in the tumor area at 4 h was 1.5 times as high as that of preinjection. These results proved that the obtained PMPDA NPs could be used as promising contrast agents for MRI application.

3.3. Assement of Photothermal Effect in Vitro.

Nonpolymeric dopamine has no absorption in the NIR region and cannot be used for photothermal ablation. On the contrary, an important feature of polydopamine nanomaterials is their strong optical absorption from ultraviolet (UV) to NIR regions.[15] The vis–NIR spectra of PDA, Mn^{2+}–PDA, and PMPDA NPs are displayed in Figure 5a. PDA nanoparticles dispersed in aqueous solution exhibited broad absorption in the range of 400–900 nm. The molar extinction coefficient of 160 nm PMPDA nanoparticles was as high as 1.24×10^{10} M^{-1} cm^{-1}. And this value was comparable to that of gold nanoshell[40] (1.4×10^{11} M^{-1} cm^{-1} at 800 nm) or gold nanorods[41] (5.24×10^{9} M^{-1} cm^{-1} at 808 nm). After the chelation of Mn^{2+} ions or SH-PEG modification, the optical absorption had a slight change in the range of 700–900 nm. Furthermore, the absorbance at 808 nm linearly increased with the increase of PMPDA concentration in aqueous solution (Figure S3), also proving that PMPDA NPs dispersed very well in water. The strong absorbance in the NIR region and good colloidal stability suggested the potential of PMPDA NPs as a photothermal agent to convert NIR light energy to heat energy.

To evaluate the photothermal effect induced by NIR irradiation, different concentrations of PMPDA suspensions in a quartz well were exposed to an 808 nm laser with an output power of 2 W for 10 min. Deionized water was used as a negative control. The temperature elevation during irradiation is shown in Figure 5b. All the PMPDA samples showed dramatic temperature elevation, while no significant temperature change was observed for deionized water. After the irradiation, the temperature of PMPDA suspensions with a concentration of 100 μg/mL raised from 25.5 to 50.1 °C (an increase of 24.6 °C), which is sufficient to induce irreversible cell death.[16] Besides, the temperature change of PDA or Mn^{2+}–PDA suspensions with a concentration of 100 μg/mL was almost the same as that of PMPDA suspensions (Figure S4) under the identical condition, coinciding with their almost equal absorbance at 808 nm. The localized photothermal killing of cancer cells was further performed. HeLa cells were incubated with 100 μg/mL PMPDA NP dispersions for 4 h in a six-well plate and then irradiated using a NIR laser (808 nm, 6 W cm^{-2}) for 10 min. After the treatment, calcein AM was used to stain HeLa cells for visualization of living cells. As shown in Figure 6, HeLa cells treated with either PMPDA NPs alone or laser irradiation alone showed vivid green fluorescence, indicating no apparent cell death. On the contrary, the laser illumination zone became dark when HeLa cells were treated with PMPDA NPs along with laser irradiation, indicating apparent cell death upon irradiation. The dark region was a little bigger than the illumination zone because of the effect of heat transferring to surrounding environment. Then we further quantitatively evaluated the photothermal cytotoxicity of PMPDA NPs on HeLa cells using a standard MTT (3-(4, 5-dimethylthiazol-2-yl)-2,5-diphenyltetrazolium bromide) assay. HeLa cells were incubated with different concentration of PMPDA NPs for 4 h. Upon laser irradiation for 10 min, the cell viability of HeLa cells significantly decreased with increasing

DOI: 10.1021/acsami.5b06265
ACS Appl. Mater. Interfaces 2015, 7, 16946–16952

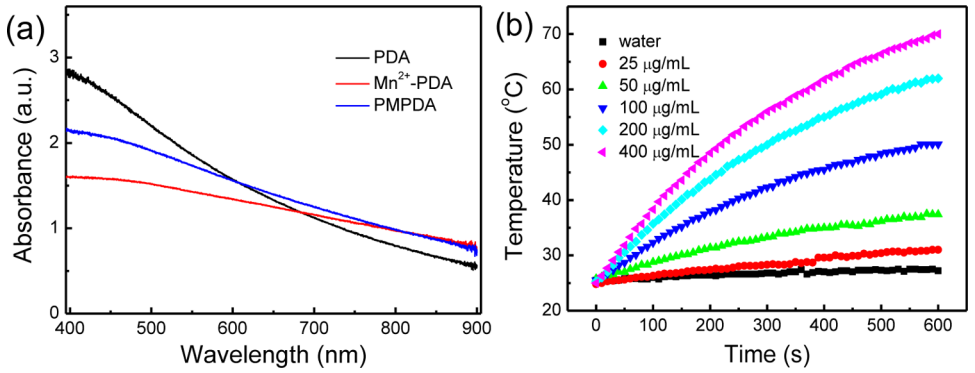

Figure 5. (a) Visible−NIR absorption spectra of PDA NPs, Mn^{2+}−PDA NPs, and PMPDA NPs. (b) Temperature elevation of water and different concentrations of PMPDA NPs suspensions as a function of irradiation time upon exposure to NIR light.

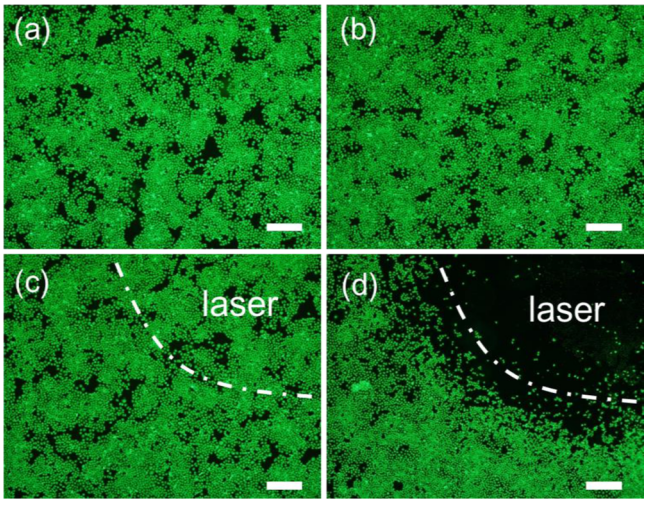

Figure 6. Fluorescence microscopy images of HeLa cells stained with calcein AM after different treatments: (a) without laser irradiation or PMPDA NPs; (b) with 100 μg/mL PMPDA NPs only; (c) with 10 min of laser irradiation only; (d) with both 100 μg/mL PMPDA NPs and 10 min of laser irradiation. Scale bars are 500 μm.

concentrations of PMPDA NPs, and less than 16% of HeLa cells remained alive at the concentration of 80 μg/mL (see Figure 7a). These results proved that PMPDA NPs could be used as effective photothermal agents for cancer treatment.

3.4. Assement of Cytotoxicity. The ideal theranostic agents should be nontoxic or have low toxicity for biomedical applications. To study the potential cytotoxicity of PMPDA NPs, human umbilical vein endothelial cells (HUVECs) were used as model cells and a standard MTT assay was also conducted. Quantitative evaluation results showed that the cytotoxicity of PMPDA NPs was concentration-dependent, and more than 95% of HUEVCs remained alive after a 24 h exposure to PMPDA NPs with concentration as high as 320 μg mL^{-1} (Figure 7b), indicating excellent biocompatibility and low toxicity of PMPDA NPs, which was in accordance with that of PDA nanoparticles as previously reported.[17] At the concentration of 80 μg/mL, about 99% of HUEVCs remained alive after a 24 h exposure to PMPDA NPs while less than 16% of HeLa cells remained alive upon laser irradiation for 10 min. Considering both the treatment of photothermal ablation and potential cytotoxicity, the optimal concentration for phtothermal ablation of HeLa cells should be 80 μg/mL. The excellent biocompatibility of PMPDA NPs ensures the safety of further applications in biomedicine field.

4. CONCLUSIONS

In summary, PMPDA nanoparticles have been successfully developed as novel theranostic agents via introducing Mn^{2+} and SH-PEG onto PDA nanoparticles without the assistance of any extrinsic chelators. The as-prepared PMPDA nanoparticles show significant MRI signal enhancement for both in vitro and in vivo imaging because of intrinsic manganese-chelating properties, and the value of longitudinal relaxivity coefficient is as high as 6.55 mM^{-1} s^{-1} at 9.4 T. In addition, PMPDA nanoparticles can kill cancer cells effectively because of obvious photothermal effects. Importantly, the fabrication procedure was very simple and safe, and the use of Mn^{2+} ions as contrast

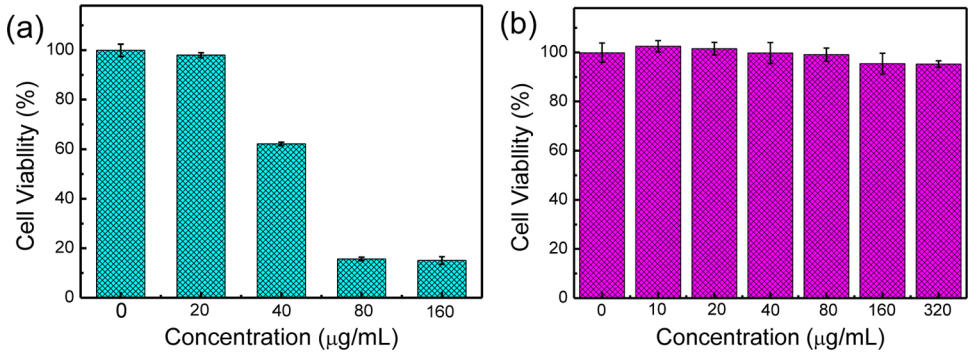

Figure 7. (a) Cell viability of HeLa cells exposed to different concentrations of PMPDA nanoparticles with laser irradiation for 10 min. (b) Cell viability of HUVECs exposed to different concentrations of PMPDA nanoparticles for 24 h.

DOI: 10.1021/acsami.5b06265
ACS Appl. Mater. Interfaces 2015, 7, 16946−16952

agents and biodegradable polydopamine as photothermal agents can decrease the toxicity of PMPDA nanoparticles, ensuring their superiority over other theranostic agents for MRI-guided phototherapy. Hence, the biocompatible PMPDA nanoparticles could be used as promising platforms for MRI-guided photothermal therapy of cancer cells.

■ ASSOCIATED CONTENT

Supporting Information

The Supporting Information is available free of charge on the ACS Publications website at DOI: 10.1021/acsami.5b06265.

Additional TEM images, FTIR spectra, and temperature elevation of PDA, Mn^{2+}–PDA, and PMPDA nanoparticles solutions, stability study of PMPDA nanoparticles, and the relaxivity coefficients of PMPDA nanoparticles at 1.5 T (PDF)

■ AUTHOR INFORMATION

Corresponding Author

*E-mail: cy_xu@hit.edu.cn.

Notes

The authors declare no competing financial interest.

■ ACKNOWLEDGMENTS

This work was supported by the Fundamental Research Funds for the Central Universities (Grant HIT.BRETIII.201203). The authors thank the Center for Molecular Imaging and Translational Medicine in Xiamen University for MR imaging in vivo.

■ REFERENCES

(1) Jokerst, J. V.; Gambhir, S. S. Molecular Imaging with Theranostic Nanoparticles. *Acc. Chem. Res.* **2011**, *44*, 1050–1060.

(2) Ke, H.; Wang, J.; Dai, Z.; Jin, Y.; Qu, E.; Xing, Z.; Guo, C.; Yue, X.; Liu, J. Gold-Nanoshelled Microcapsules: A Theranostic Agent for Ultrasound Contrast Imaging and Photothermal Therapy. *Angew. Chem., Int. Ed.* **2011**, *50*, 3017–3021.

(3) Seo, W. S.; Lee, J. H.; Sun, X.; Suzuki, Y.; Mann, D.; Liu, Z.; Terashima, M.; Yang, P. C.; McConnell, M. V.; Nishimura, D. G. FeCo/Graphitic-Shell Nanocrystals as Advanced Magnetic-Resonance-Imaging and Near-Infrared Agents. *Nat. Mater.* **2006**, *5*, 971–976.

(4) Wang, C.; Chen, J.; Talavage, T.; Irudayaraj, J. Gold Nanorod/Fe_3O_4 Nanoparticle "Nano-Pearl-Necklaces" for Simultaneous Targeting, Dual-Mode Imaging, and Photothermal Ablation of Cancer Cell. *Angew. Chem., Int. Ed.* **2009**, *48*, 2759–2763.

(5) Yang, K.; Hu, L.; Ma, X.; Ye, S.; Cheng, L.; Shi, X.; Li, C.; Li, Y.; Liu, Z. Multimodal Imaging Guided Photothermal Therapy using Functionalized Graphene Nanosheets Anchored with Magnetic Nanoparticles. *Adv. Mater.* **2012**, *24*, 1868–1872.

(6) Jori, G.; Spikes, J. D. Photothermal Sensitizers: Possible Use in Tumor Therapy. *J. Photochem. Photobiol., B* **1990**, *6*, 93–101.

(7) Chou, S.-W.; Shau, Y.-H.; Wu, P.-C.; Yang, Y.-S.; Shieh, D.-B.; Chen, C.-C. In Vitro and In Vivo Studies of FePt Nanoparticles for Dual Modal CT/MRI Molecular Imaging. *J. Am. Chem. Soc.* **2010**, *132*, 13270–13278.

(8) Li, Z.; Zeng, Y.; Zhang, D.; Wu, M.; Wu, L.; Huang, A.; Yang, H.; Liu, X.; Liu, J. Glypican-3 Antibody Functionalized Prussian Blue Nanoparticles for Targeted MR Imaging and Photothermal Therapy of Hepatocellular Carcinoma. *J. Mater. Chem. B* **2014**, *2*, 3686–3696.

(9) Zhang, S.; Zha, Z.; Yue, X.; Liang, X.; Dai, Z. Gadolinium-Chelate Functionalized Copper Sulphide as A Nanotheranostic Agent for MR Imaging and Photothermal Destruction of Cancer Cells. *Chem. Commun.* **2013**, *49*, 6776–6778.

(10) Zha, Z.; Yue, X.; Ren, Q.; Dai, Z. Uniform Polypyrrole Nanoparticles with High Photothermal Conversion Efficiency for Photothermal Ablation of Cancer Cells. *Adv. Mater.* **2013**, *25*, 777–782.

(11) Xiao, J.; Tian, X.; Yang, C.; Liu, P.; Luo, N.; Liang, Y.; Li, H.; Chen, D.; Wang, C.; Li, L. Ultrahigh Relaxivity and Safe Probes of Manganese Oxide Nanoparticles for *In Vivo* Imaging. *Sci. Rep.* **2013**, *3*, 3424.

(12) Kim, T.; Momin, E.; Choi, J.; Yuan, K.; Zaidi, H.; Kim, J.; Park, M.; Lee, N.; McMahon, M. T.; Quinones-Hinojosa, A. Mesoporous Silica-Coated Hollow Manganese Oxide Nanoparticles as Positive T_1 Contrast Agents for Labeling and MRI Tracking of Adipose-Derived Mesenchymal Stem Cells. *J. Am. Chem. Soc.* **2011**, *133*, 2955–2961.

(13) Lee, T.; Bang, D.; Park, Y.; Kim, S. H.; Choi, J.; Park, J.; Kim, D.; Kim, E.; Suh, J. S.; Huh, Y. M. Gadolinium-Enriched Polyaniline Particles (GPAPs) for Simultaneous Diagnostic Imaging and Localized Photothermal Therapy of Epithelial Cancer. *Adv. Healthcare Mater.* **2014**, *3*, 1408–1414.

(14) MacDonald, T. D.; Liu, T. W.; Zheng, G. An MRI-Sensitive, Non-Photobleachable Porphysome Photothermal Agent. *Angew. Chem., Int. Ed.* **2014**, *53*, 6956–6959.

(15) Liu, Y.; Ai, K.; Lu, L. Polydopamine and Its Derivative Materials: Synthesis and Promising Applications in Energy, Environmental, and Biomedical Fields. *Chem. Rev.* **2014**, *114*, 5057–5115.

(16) Hirsch, L. R.; Stafford, R.; Bankson, J.; Sershen, S.; Rivera, B.; Price, R.; Hazle, J.; Halas, N.; West, J. L. Nanoshell-mediated Near-Infrared Thermal Therapy of Tumors Under Magnetic Resonance Guidance. *Proc. Natl. Acad. Sci. U. S. A.* **2003**, *100*, 13549–13554.

(17) Liu, Y.; Ai, K.; Liu, J.; Deng, M.; He, Y.; Lu, L. Dopamine-Melanin Colloidal Nanospheres: An Efficient Near-Infrared Photothermal Therapeutic Agent for *In Vivo* Cancer Therapy. *Adv. Mater.* **2013**, *25*, 1353–1359.

(18) Lin, L.-S.; Cong, Z.-X.; Cao, J.-B.; Ke, K.-M.; Peng, Q.-L.; Gao, J.; Yang, H.-H.; Liu, G.; Chen, X. Multifunctional Fe_3O_4@Polydopamine Core–Shell Nanocomposites for Intracellular mRNA Detection and Imaging-Guided Photothermal Therapy. *ACS Nano* **2014**, *8*, 3876–3883.

(19) Yeroslavsky, G.; Richman, M.; Dawidowicz, L.; Rahimipour, S. Sonochemically Produced Polydopamine Nanocapsules with Selective Antimicrobial Activity. *Chem. Commun.* **2013**, *49*, 5721–5723.

(20) Hung, Y.-C.; Sava, V. M.; Juang, C.-L.; Yeh, T.-C.; Shen, W.-C.; Huang, G. S. Gastrointestinal Enhancement of MRI with Melanin Derived from Tea Leaves (Thea Sinensis Linn.). *J. Ethnopharmacol.* **2002**, *79*, 75–79.

(21) Ju, K.-Y.; Lee, J. W.; Im, G. H.; Lee, S.; Pyo, J.; Park, S. B.; Lee, J. H.; Lee, J.-K. Bio-Inspired, Melanin-Like Nanoparticles as a Highly Efficient Contrast Agent for T_1-Weighted Magnetic Resonance Imaging. *Biomacromolecules* **2013**, *14*, 3491–3497.

(22) Tian, Q.; Hu, J.; Zhu, Y.; Zou, R.; Chen, Z.; Yang, S.; Li, R.; Su, Q.; Han, Y.; Liu, X. Sub-10 nm Fe_3O_4@$Cu_{2-x}S$ Core–Shell Nanoparticles for Dual-Modal Imaging and Photothermal Therapy. *J. Am. Chem. Soc.* **2013**, *135*, 8571–8577.

(23) Zeng, Y.; Zhang, D.; Wu, M.; Liu, Y.; Zhang, X.; Li, L.; Li, Z.; Han, X.; Wei, X.; Liu, X. Lipid-AuNPs@ PDA Nanohybrid for MRI/CT Imaging and Photothermal Therapy of Hepatocellular Carcinoma. *ACS Appl. Mater. Interfaces* **2014**, *6*, 14266–14277.

(24) Yu, J.; Yang, C.; Li, J.; Ding, Y.; Zhang, L.; Yousaf, M. Z.; Lin, J.; Pang, R.; Wei, L.; Xu, L. Multifunctional Fe_5C_2 Nanoparticles: A Targeted Theranostic Platform for Magnetic Resonance Imaging and Photoacoustic Tomography-Guided Photothermal Therapy. *Adv. Mater.* **2014**, *26*, 4114–4120.

(25) Yan, J.; Yang, L.; Lin, M. F.; Ma, J.; Lu, X.; Lee, P. S. Polydopamine Spheres as Active Templates for Convenient Synthesis of Various Nanostructures. *Small* **2013**, *9*, 596–603.

(26) Lydén, A.; Larsson, B. S.; Lindquist, N. G. Melanin Affinity of Manganese. *Acta Pharmacol. Toxicol.* **1984**, *55*, 133–138.

(27) Lee, H.; Dellatore, S. M.; Miller, W. M.; Messersmith, P. B. Mussel-inspired Surface Chemistry for Multifunctional Coatings. *Science* **2007**, *318*, 426–430.

DOI: 10.1021/acsami.5b06265
ACS Appl. Mater. Interfaces 2015, 7, 16946–16952

(28) Xu, L. Q.; Yang, W. J.; Neoh, K.-G.; Kang, E.-T.; Fu, G. D. Dopamine-induced Reduction and Functionalization of Graphene Oxide Nanosheets. *Macromolecules* **2010**, *43*, 8336−8339.
(29) Ahire, J. H.; Chambrier, I.; Mueller, A.; Bao, Y.; Chao, Y. Synthesis of d-Mannose Capped Silicon Nanoparticles and Their Interactions with MCF-7 Human Breast Cancerous Cells. *ACS Appl. Mater. Interfaces* **2013**, *5*, 7384−7391.
(30) Yu, M.; Niu, Y.; Yang, Y.; Hartono, S. B.; Yang, J.; Huang, X.; Thorn, P.; Yu, C. An Approach to Prepare Polyethylenimine Functionalized Silica-Based Spheres with Small Size for siRNA Delivery. *ACS Appl. Mater. Interfaces* **2014**, *6*, 15626−15631.
(31) Hayashi, K.; Nakamura, M.; Sakamoto, W.; Yogo, T.; Miki, H.; Ozaki, S.; Abe, M.; Matsumoto, T.; Ishimura, K. Superparamagnetic Nanoparticle Clusters for Cancer Theranostics Combining Magnetic Resonance Imaging and Hyperthermia Treatment. *Theranostics* **2013**, *3*, 366.
(32) França, Á.; Pelaz, B.; Moros, M.; Sánchez-Espinel, C.; Hernández, A.; Fernández-López, C.; Grazu, V.; de la Fuente, J. M.; Pastoriza-Santos, I.; Liz-Marzán, L. M. Sterilization Matters: Consequences of Different Sterilization Techniques on Gold Nanoparticles. *Small* **2010**, *6*, 89−95.
(33) Liu, X.; Cao, J.; Li, H.; Li, J.; Jin, Q.; Ren, K.; Ji, J. Mussel-inspired Polydopamine: A Biocompatible and Ultrastable Coating for Nanoparticles *In Vivo*. *ACS Nano* **2013**, *7*, 9384−9395.
(34) Jiang, J.; Zhu, L.; Zhu, L.; Zhu, B.; Xu, Y. Surface Characteristics of A Self-polymerized Dopamine Coating Deposited on Hydrophobic Polymer Films. *Langmuir* **2011**, *27*, 14180−14187.
(35) Coughlin, A. J.; Ananta, J. S.; Deng, N.; Larina, I. V.; Decuzzi, P.; West, J. L. Gadolinium-Conjugated Gold Nanoshells for Multimodal Diagnostic Imaging and Photothermal Cancer Therapy. *Small* **2014**, *10*, 556−565.
(36) Kueny-Stotz, M.; Garofalo, A.; Felder-Flesch, D. Manganese-Enhanced MRI Contrast Agents: From Small Chelates to Nanosized Hybrids. *Eur. J. Inorg. Chem.* **2012**, *2012*, 1987−2005.
(37) Rodríguez, E.; Roig, A.; Molins, E.; Arús, C.; Quintero, M. R.; Cabañas, M. E.; Cerdán, S.; Lopez-Larrubia, P.; Sanfeliu, C. *In Vitro* Characterization of An Fe_8 Cluster As Potential MRI Contrast Agent. *NMR Biomed.* **2005**, *18*, 300−307.
(38) Caravan, P.; Farrar, C. T.; Frullano, L.; Uppal, R. Influence of Molecular Parameters And Increasing Magnetic Field strength on Relaxivity of Gadolinium- and Manganese- based T_1 Contrast Agents. *Contrast Media Mol. Imaging* **2009**, *4*, 89−100.
(39) Caravan, P. Strategies for Increasing The Sensitivity of Gadolinium Based MRI Contrast Agents. *Chem. Soc. Rev.* **2006**, *35*, 512−523.
(40) Lu, W.; Huang, Q.; Ku, G.; Wen, X.; Zhou, M.; Guzatov, D.; Brecht, P.; Su, R.; Oraevsky, A.; Wang, L. V. Photoacoustic Imaging of Living Mouse Brain Vasculature Using Hollow Gold nanospheres. *Biomaterials* **2010**, *31*, 2617−2626.
(41) Fu, G.; Liu, W.; Feng, S.; Yue, X. Prussian Blue Nanoparticles Operate as A New Generation of Photothermal Ablation Agents for Cancer Therapy. *Chem. Commun.* **2012**, *48*, 11567−11569.

DOI: 10.1021/acsami.5b06265
ACS Appl. Mater. Interfaces 2015, 7, 16946−16952